JOC*Article*

Multidimensional Tunneling in the [1,5] Shift in (*Z*)-1,3-Pentadiene: How Useful Are Swain−Schaad Exponents at Detecting Tunneling?

Dana N. Peles and John D. Thoburn*

Department of Chemistry, Randolph-Macon College, Ashland, Virginia 23005

jthoburn@rmc.edu

Received December 14, 2007

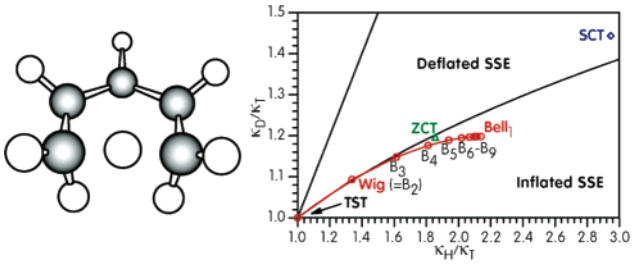

Rates, kinetic isotope effects (KIE), and Swain−Schaad exponents (SSE) have been calculated for a variety of isotopologues for the [1,5] shift in (*Z*)-1,3-pentadiene using mPW1K/6-31+G(d,p). Quantum mechanical effects along the reaction coordinate were incorporated with the zero-curvature tunneling (ZCT) model and with the multidimensional small curvature tunneling (SCT) model, which allows for coupling of modes perpendicular to the reaction coordinate. The latter model gives the best agreement with experimental rates and primary KIEs. The small quasiclassical primary KIE (2.6) is rationalized in terms of a nonlinear transition state. For sp^3 to sp^2 rehybridization, the quasiclassical α-secondary KIE shows an unusual inverse effect due to compression of the nonbonding hydrogens in the suprafacial transition state. SCT transmission coefficients (κ) increase the rates by as much as one order of magnitude. Tunneling allows the reactant to evade 1−2.5 kcal/mol of the barrier depending on the isotope. Inclusion of tunneling in the secondary KIE increases it beyond the equilibrium isotope effect and converts the inverse effect (0.95) into a normal KIE (1.12). Tunneling was found to deflate the primary *y* SSE but by an amount too small to distinguish it from the quasiclassical SSE. On the other hand, when a specific labeling pattern is used, the difference between the quasiclassical secondary SSE (4.1) and the tunneling secondary SSE (2.3) may be sufficiently large to detect tunneling. The mixed secondary SSE shows even larger differences.

Introduction

Quantum mechanical tunneling[1] (QMT) through a barrier is an intriguing yet widespread aspect of many chemical reactions involving light atoms, but often the extent of tunneling is difficult to quantify. For example, Doering has recently concluded that tunneling is not important in the [1,5] hydrogen shift[2] despite a variety of calculations to the contrary.[3,4] It has been further suggested that an excellent agreement between the B3LYP/6-31G(d) nontunneling activation enthalpies and the experimental barrier implies either a fortuitous coincidence or the absence of significant tunneling in the [1,5] shift.[5] The purpose of this paper is twofold: first, to re-examine the experimental data in light of multidimensional tunneling calculations at a high level of theory, and second, to investigate

(1) Bell, R. P. *The Tunneling Effect in Chemistry*; Chapman and Hall: New York, 1980.

(2) Doering, W. v. E.; Zhao, X. *J. Am. Chem. Soc.* **2006**, *128*, 9080.

(3) (a) Bingham, R. C.; Dewar, M. J. S. *J. Am. Chem. Soc*. **1972**, *94*, 9107; Dewar, M. J. S.; Merz, K. M., Jr.; Stewart, J. J. P. *J. Chem. Soc. Chem Comm*. **1985**, 166; Dewar, M. J. S.; Healy, E. F.; Ruiz, J. M. *J. Am. Chem. Soc*. **1988**, *110*, 2666. (b) Hess, B. A., Jr.; Schaad, L. J.; Pancir, J. *J. Am. Chem. Soc*. **1985**, *107*, 149. (c) Dormans, G. J. M.; Buck, H. M. *J. Am. Chem. Soc*. **1986**, *108*, 3253. (d) Jensen, F.; Houk, K. N. *J. Am. Chem. Soc*. **1987**, *109*, 3139. (e) Chantranupong, L.; Wildman, T. A. *J. Am. Chem. Soc*. **1990**, *112*, 4151.

(4) Liu, Y.-P.; Lynch, G. C.; Truong, T. N.; Lu, D.-H.; Truhlar, D. G.; Garrett, B. C. *J. Am. Chem. Soc*. **1993**, *115*, 2408.

(5) Hayase, S.; Hrovat, D. A.; Borden, W. T. *J. Am. Chem. Soc*. **2004**, *126*, 10028.

10.1021/jo702668u CCC: $40.75
Published on Web 03/26/2008

whether Swain−Schaad exponents would be a reliable test for the presence of tunneling in this reaction.

Many tests for quantum tunneling have been devised:[6] kinetic isotope effects (KIEs, e.g., k_H/k_D) that exceed the quasiclassical[7] maximum, temperature-independent KIEs, isotope-induced deviations in the Arrhenius parameters (A_H/A_D or $E_a^D - E_a^H$), and deviations from the quasiclassical Swain−Schaad exponents (SSE). The Swain−Schaad relationship was initially used to estimate an isotope's effect on a reaction rate when the rates are known for two other isotopologues; thus, if one knows k_H/k_D, one can estimate k_T based on the known reduced masses.[8] The SSE is defined as the ratio of logarithms of the KIEs according to either eq 1[8] or eq 2:[9]

$$x = \frac{\ln(k_H/k_T)}{\ln(k_H/k_D)} \quad (1)$$

$$y = \frac{\ln(k_H/k_T)}{\ln(k_D/k_T)} \quad (2)$$

The magnitude of the SSE ($x \approx 1.4$, $y \approx 3.3$)[9] is thought to be more or less invariant when the SSE is derived from primary KIEs. Factors such as tunneling along the reaction coordinate and variational effects can perturb the primary SSE, but the effects tend to be small and often cancel, thereby making deviations from the primary SSE not a generally useful test for tunneling.[10−12] Equations 1 and 2 can also be used with secondary KIEs, but the secondary quasiclassical exponents x and y are no longer guaranteed to fall in a narrow, well-defined range when the KIE itself is close to unity.[13] One may further define "mixed" SSEs in which isotopic substitution occurs at both the primary and secondary positions, e.g.

$$\text{secondary } y^{mix} = \frac{\ln(k_{HH}/k_{HT})}{\ln(k_{DD}/k_{DT})} \quad (3)$$

in which i is the transferred isotope and j is the nontransferred isotope in k_{ij}. When the stretching motion of the primary site couples strongly with the bending motion of the secondary site, the mixed SSE is inflated due to a breakdown in the rule of the geometrical mean,[14] and a maximum quasiclassical value of 4.8 has been proposed.[15] Oxidation of benzyl alcohol with a variety of alcohol dehydrogenases show a wide range of secondary mixed SSE ($3.3 <$ secondary $y^{mix} < 10.2$).[16] Initially, these large SSEs were attributed to tunneling, but it is now believed that dynamic motion of the protein works in conjunction with tunneling to give such large SSEs.[17,18] It appears that only the mixed secondary SSE is suitable for detecting tunneling[19] and even then it is not guaranteed because factors, such as the kinetic complexity associated with substrate binding and product release in enzymatic reactions, can decrease the SSE and mask the presence of tunneling.[20] Treating tunneling as a nonadiabatic transition between localized diabatic proton vibrational levels, Hynes calculates that the Swain−Schaad ratio may reflect quantum tunneling depending on temperature regime and reaction asymmetry.[21]

Much of the computational effort in this area has focused on defining the quasiclassical range for the SSE. Our approach here is not to seek a universal "normal" or "abnormal" range for the SSE, but rather to calculate the transmission coefficients with and without tunneling to determine how tunneling affects the magnitude of the SSE for specific reactions. For this initial study we have selected a simple prototypical reaction free of kinetic complexity, but not necessarily tunneling, namely the degenerate [1,5] hydrogen shift in (*Z*)-1,3-pentadiene. As the paradigm of the concerted sigmatropic reaction, there have been both experimental[22] and computational studies of 1,3-pentadiene[23] and its derivatives.[2,5,23] Truhlar has already demonstrated the validity of the variational transition state theory (VTST) with the multidimensional tunneling (MDT) approach using semiempirical potentials for the title reaction.[4] In a recent study on the [1,5] shift in 5-methyl-1,3-cyclopentadiene, Borden concluded that the SSE is only useful at detecting tunneling when measured over a broad temperature range.[24]

In this study we calculate the effect of multidimensional tunneling on the α-secondary KIEs and associated Swain−Schaad exponents for the [1,5] shift in (*Z*)-1,3-pentadiene using a variety of isotopologues:

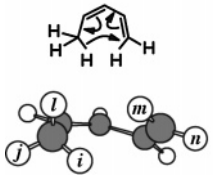

i	*j*	*l*	*m*	*n*
H	H	H	H	H
D	H	H	H	H
T	H	H	H	H
D	D	D	H	H
H	D	D	H	H
H	T	T	H	H
D	T	T	H	H

Computational Section

Methods. Rate constants were calculated using variational transition state theory (VTST) with multidimensional tunneling

(6) Kim, Y.; Kreevoy, M. M. *J. Am. Chem. Soc.* **1992**, *114*, 7116.
(7) For the distinction between quasiclassical and semiclassical see ref 18.
(8) Swain, C. G.; Stivers, E. C.; Reuwer, J. F.; Schaad, L. J. *J. Am. Chem. Soc.* **1958**, *80*, 5885.
(9) Streitwieser, A., Jr.; Hollyhead, W. B.; Pudjaatmaka, A. H.; Owens, P. H.; Kruger, T. L.; Rubenstein, P. A.; MacQuarrie, R. A.; Brokaw, M. L.; Chu, W. K. C.; Niemeyer, H. M. *J. Am. Chem. Soc.* **1971**, *93*, 5088.
(10) Tautermann, C. S.; Loferer, M. J.; Voegele, A. F.; Liedl, K. R. *J. Chem. Phys.* **2004**, *120*, 11650. Note that the formic acid dimers in this study lack *secondary* hydrogens, and the SSE arising from substitution at secondary sites are more sensitive to tunneling.
(11) Smedarchina, Z.; Siebrand, W. *Chem. Phys. Lett.* **2005**, *410*, 370.
(12) Cui, Q.; Karplus, M. *J. Am. Chem. Soc.* **2002**, *124*, 3093.
(13) Hirschi, J.; Singleton, D. A. *J. Am. Chem. Soc.* **2005**, *127*, 3294.
(14) Bigeleisen, J. *J. Chem. Phys.* **1955**, *23*, 2264.
(15) Kohen, A.; Jensen, J. H. *J. Am. Chem. Soc.* **2002**, *124*, 3858. Kohen, A. In *Isotope Effects in Chemistry and Biology*; Kohen, A., Limbach, H.-H., Eds.; Taylor and Francis: Boca Raton, FL, 2006; p 915.
(16) (a) Cha, Y.; Murray, C. J.; Klinman, J. P. *Science* **1989**, *243*, 1325. (b) Bahnson, B. J.; Park, D.-H.; Kim, K.; Plapp, B. V.; Klinman, J. P. *Biochem.* **1993**, *32*, 5503. (c) Bahnson, N. J.; Colby, T. D.; Chin, J. K.; Goldstein, B. M.; Klinman, J. P. *Proc. Natl. Acad. Sci., U.S.A.* **1997**, *94*, 12797.
(17) Nagel, Z. D.; Klinman, J. P. *Chem. Rev.* **2006**, *106*, 3095.
(18) Alhambra, C.; Corchado, J. C.; Sanchez, M. L.; Garcia-Viloca, M.; Gao, J.; Truhlar, D. G. *J. Phys. Chem. B* **2001**, *105*, 11326.
(19) Saunders, W. H. *J. Am. Chem. Soc.* **1985**, *107*, 164. Amin, M.; Price, R. C.; Saunders, W. H. *J. Am. Chem. Soc.* **1990**, *112*, 4467. Huskey, W. P. *J. Phys. Org. Chem.* **1991**, *4*, 361. Grant, K. L.; Klinman, J. P. *Bioorg. Chem.* **1992**, *20*, 1.
(20) Kohen, A.; Klinman, J. P. *Chem. Biol.* **1999**, *6*, R191.
(21) Kiefer, P. M.; Hynes, J. T. *J. Phys. Chem. A* **2004**, *108*, 11793.
(22) Roth, W. R.; König, J. *Liebigs Ann. Chem.* **1966**, *699*, 24.
(23) Hess, B. A.; Baldwin, J. E. *J. Org. Chem.* **2002**, *76*, 6025.
(24) Shelton, G. R.; Hrovat, D. A.; Borden, W. T. *J. Am. Chem. Soc.* **2007**, *129*, 164. Shelton, G. R.; Hrovat, D. A.; Borden, W. T. *J. Am. Chem. Soc.* **2007**, *129*, 16115.

(MDT). Excellent reviews on this subject are available,[25] and a brief summary is provided in the Supporting Information. We focus here on the details of the tunneling methods that are important in this work.

There is a finite probability that reactants with an energy less than that necessary to surmount the saddle point will nevertheless cross to products via an incoherent tunneling process when the barrier width is comparable to the de Broglie wavelength of the transferred particle. Computationally, tunneling can be incorporated into the transmission coefficient (κ), which is related to the tunneling probabilities. The transmission coefficient is the ratio of quantum mechanical and classical thermally averaged transmission probabilities

$$\kappa(T) = \frac{\int_0^\infty P(E)e^{-\beta E}\mathrm{d}E}{\int_{V_a^G}^\infty e^{-\beta E}\mathrm{d}E} = \beta e^{-\beta V a^G}\int_0^\infty P(E)e^{-\beta E}\mathrm{d}E \qquad (4)$$

where V_a^G is the barrier height and $P(E)$ is the probability that reactants will cross to products. For those reactants with an energy less than V_a^G, the transmission probabilities can be approximated using the semiclassical WKB approximation for a smooth potential

$$P(E) = \frac{1}{1 + e^{2\theta}} \qquad (5)$$

where θ is the imaginary-action integral that describes how much the wavefunction is dampened by the potential barrier

$$\theta(E) = \frac{1}{\hbar}\int_{s<}^{s>} \sqrt{2\mu(V(s) - E)}\,\mathrm{d}s \qquad (6)$$

The limits of the integral are the classical turning points of the tunneling path, that is, the location of the pre- and post-tunneling geometries, while μ is the reduced mass. Thus, to calculate a transmission coefficient, one has to integrate the tunneling momentum for a given tunneling path at a specific energy, which is used to calculate energy dependent transmission probabilities, and finally integrate the transmission probabilities over all possible energies available to the molecule.

The extent of tunneling is highly dependent on the barrier shape, with narrow barriers enhancing tunneling. For simplicity one could approximate a barrier as a parabola whose width is determined by the transition-state imaginary frequency. A more accurate barrier however is the minimum energy path (MEP) that connects reactants, transition state, and products. Such an MEP can be constructed using electronic structure methods. This one-dimensional, "zero-curvature" model (ZCT) assumes that tunneling takes place only along the MEP. However, other tunnel paths are possible. When the reaction coordinate couples to orthogonal vibrational modes, the tunnel path is effectively shortened and tunneling enhanced. This shortened path occurs on the concave side of the MEP and therefore is called "corner-cutting". If the deviations from the MEP are not large (small-curvature tunneling, or SCT), the potential energy surface (PES) in the vicinity of the MEP can be approximated from the vibrational modes orthogonal to the MEP. Operationally, the dampening of the wavefunction, $\theta^{SCT}(T)$, is calculated by replacing the reduced mass, μ, of eq 6 with an effective reduced mass, μ_{eff}, which is determined by the local curvature along the MEP. The effect of the reaction path curvature is to lower the effective mass and raise the tunneling probability. Note that the SCT method does not actually calculate additional trajectories in the vicinity of the transition state but calculates the transmission coefficient based on the properties associated with the MEP. Large curvature tunneling (LCT) can occur when the skew angle for the reaction path is unusually small, in which case the assumptions of the SCT method no longer hold. For the [1,5] shift in pentadiene, however, it was found that the LCT method did not increase transmission coefficients beyond SCT, indicating that large curvature tunneling is not operative in this reaction.

Details. Rate constants were calculated using POLYRATE9.4,[26] which calculates rates based on a reaction path generated by GAUSSRATE9.1,[27] which in turn gets path information (geometries, energies, gradients, and Hessian) from GAUSSIAN03.[28] The potentials were generated with the mPW1K hybrid DFT method and 6-31+G(d,p) basis set. This relatively inexpensive method has been shown to provide highly accurate barrier heights.[29] Houk has demonstrated the convergence of the mPW1K method with both the CBS-QB3 method and experiment.[30]

All stationary points were optimized using GAUSSIAN03 to confirm geometries and number of imaginary frequencies: zero for reactants and products, one for the saddle point. All vibrational modes were calculated using the harmonic approximation with a scaling 0.9515.[29b] Since the experimental kinetics were measured in the gas phase, there is no need to make additional solvent corrections to the calculations. The rate constants for the hydrogen transfer step, as determined by POLYRATE, were multiplied by a temperature- and isotope-dependent equilibrium constant to include the effects of the rapid pre-equilibrium between the unreactive s-trans and the reactive s-cisoid conformers. Because the MEP is mass dependent each isotope has a unique MEP. Given the expense associated with the MEP calculation, it is desirable to use an alternative method in which one can approximate the rate for any isotopologue from a single reaction path by variationally reorienting the dividing surface that separates reactants and products along the reaction path, as implemented by the RODS algorithm in GAUSSRATE/POLYRATE.[31]

Results

mPW1K Geometries and Conformational Analysis. The mPW1K reactant, transition state, and product geometries

(25) For reviews of VTST and MDT, see: Truhlar, D. G.; Isaacson, A. D.; Garrett, B. C. In *The Theory of Chemical Reaction Dynamics*; Baer, M., Ed.; CRC Press: Boca Raton, 1985; Vol 4, pp 65−137. Tucker, S. C.; Truhlar, D. G. In *New Theoretical Concepts for Understanding Organic Reactions*; Bertran, J.; Csizmadia, I. G., Eds.; Kluwer: Dordrecht, 1989; pp 291−346. Truhlar, D. G. In *Isotope Effects in Chemistry and Biology*; Kohen, A.; Limbach, H.-H., Eds.; CRC Press: Boca Raton, 2006; pp 579−619.

(26) Corchado, J. C.; Chuang, Y.-Y.; Fast, P. L.; Hu, W.-P.; Liu, Y.-P.; Lynch, G. C.; Nguyen, K. A.; Jackels, C. F.; Fernandez-Ramos, A.; Ellingson, B. A.; Lynch, B. J.; Melissas, V. S.; Villà, J.; Rossi, I.; Coitiño, E. L.; Pu, J.; Albu, T. V.; Steckler, R.; Garrett, B. C.; Isaacson, A. D.; Truhlar, D. G. POLYRATE version 9.4, May 2006.

(27) Corchado, J. C.; Chuang, Y.-Y.; Coitino, E. L.; Truhlar, D. G. GAUSSRATE version 9.1, July 2003.

(28) Frisch, M. J.; Trucks, G. W.; Schlegel, H. B.; Scuseria, G. E.; Robb, M. A.; Cheeseman, J. R.; Montgomery, J. A., Jr.; Vreven, T.; Kudin, K. N.; Burant, J. C.; Millam, J. M.; Iyengar, S. S.; Tomasi, J.; Barone, V.; Mennucci, B.; Cossi, M.; Scalmani, G.; Rega, N.; Petersson, G. A.; Nakatsuji, H.; Hada, M.; Ehara, M.; Toyota, K.; Fukuda, R.; Hasegawa, J.; Ishida, M.; Nakajima, T.; Honda, Y.; Kitao, O.; Nakai, H.; Klene, M.; Li, X.; Knox, J. E.; Hratchian, H. P.; Cross, J. B.; Adamo, C.; Jaramillo, J.; Gomperts, R.; Stratmann, R. E.; Yazyev, O.; Austin, A. J.; Cammi, R.; Pomelli, C.; Ochterski, J. W.; Ayala, P. Y.; Morokuma, K.; Voth, G. A.; Salvador, P.; Dannenberg, J. J.; Zakrzewski, V. G.; Dapprich, S.; Daniels, A. D.; Strain, M. C.; Farkas, O.; Malick, D. K.; Rabuck, A. D.; Raghavachari, K.; Foresman, J. B.; Ortiz, J. V.; Cui, Q.; Baboul, A. G.; Clifford, S.; Cioslowski, J.; Stefanov, B. B.; Liu, G.; Liashenko, A.; Piskorz, P.; Komaromi, I.; Martin, R. L.; Fox, D. J.; Keith, T.; Al-Laham, M. A.; Peng, C. Y.; Nanayakkara, A.; Challacombe, M.; Gill, P. M. W.; Johnson, B.; Chen, W.; Wong, M. W.; Gonzalez, C.; Pople, J. A. GAUSSIAN version 03, Gaussian, Inc., Pittsburgh, PA, 2003.

(29) (a) Lynch, B. J.; Fast, P. L.; Harris, M.; Truhlar, D. G. *J. Phys. Chem. A* **2000**, *104*, 4811. (b) Lynch, B. J.; Truhlar, D. G. *J. Phys. Chem. A* **2001**, *105*, 2936.

(30) Guner, V.; Khoung, K. S.; Leach, A. G.; Lee, P. S.; Bartberger, M. D.; Houk, K. N. *J. Phys. Chem. A* **2003**, *107*, 11445.

(31) Fast, P. L.; Corchado, J. C.; Truhlar, D. G. *J. Chem. Phys.* **1998**, *109*, 6237.

(Tables S1−S3) have slightly smaller bond distances (by 0.005−0.01 Å) and smaller bond angles (by 0−1°) than those from other DFT methods[5,32] but are still consistent with them as well as *ab initio* methods.[33] A relaxed potential energy scan was calculated for rotation about C_2-C_3 bond (Figure S1) by incrementing a locked dihedral angle while optimizing all other degrees of freedom to a minimum energy. The planar s-trans is the lowest energy conformer, but it is unreactive toward hydrogen transfer. The reactive s-cisoid is attained by rotation via a transition state in which the two π-bonds are nearly perpendicular. The s-trans/s-cisoid pre-equilibrium adds about 3.4 kcal/mol to the energy barrier, depending on temperature and isotope. The planar C_s s-cis saddle point about 0.5 kcal/mol higher in energy than the C_1 s-cisoid, indicating the barrier separating the enantiomeric s-cisoid conformers is quite small.

Barrier Heights and Rates. Barriers for the [1,5] hydrogen shift have been calculated by many methods.[5,32,33] Computational results are most accurate and useful when comparing two similar species, such as isotopologues, because systematic errors tend to cancel. Favorable agreement between calculated and experimental rates is more challenging. The CVT/SCT B3LYP/6-31G(d) rates were faster than the experimental rates, which is consistent with the known tendency of B3LYP to underestimate barrier heights.[34] The mPW1K/6-31+G(d,p) barrier heights were modestly higher than those of the B3LYP (by about 0.7 kcal/mol) and are in fact comparable to the QCISTD/6-311G(d) barrier.[33] The mPW1K method with multidimensional tunneling (SCT) brought the rates to within a factor of 4 or 5 of the experimental values: at 470 K $k_H^{calc} = 1.8 \times 10^{-5}$ s^{-1} vs $k_H^{exp} = 4 \times 10^{-6}$ s^{-1}; $k_D^{calc} = 3.9 \times 10^{-6}$ s^{-1} vs $k_D^{exp} = 8 \times 10^{-7}$ s^{-1}. Semiempirical methods (MINDO/3, AM1, and PM3) that included multidimensional tunneling[4] gave rates that varied tremendously (from 10^{-4} s^{-1} to 10^{-9} s^{-1}), but the AM1 method did particularly well (1.2×10^{-6} s^{-1}). In fact, AM1 does as well as the more sophisticated DFT method specifically optimized for kinetics, although that result may be fortuitous since it appears to overestimate the hydrogen shift barrier and underestimate the s-trans/s-cis energy difference. The key feature of the best methods appears to be the use of the multidimensional tunneling. Variational optimization of the location of the dividing surface was found to have no effect on the rate constants meaning that for this reaction the optimal dividing surface is co-incident with the traditional transition state.

Primary KIEs. Before we consider the effect of tunneling on [1,5] hydrogen shifts in depth, we must first consider both the primary and secondary quasiclassical KIEs. Each of the five terminal hydrogens in *Z*-1,3-pentadiene contributes to the rates (k_{ijlmn} where i is the transferred isotope) and the isotope effects in a complex manner (Figure 1). The calculated quasiclassical H/D primary KIEs at 450 K is only 2.6 (2.5 and 2.7 for the forward and reverse reactions, respectively, using Roth's mixed isotopologues, which have an additional α-secondary KIE). Even when corrected to 300 K, the calculated KIE (3.9) is significantly reduced from the classical maximum of about 7. Why are these quasiclassical primary KIEs so small? In the C_s symmetric suprafacial transition state, the transferred hydrogen is symmetrically placed between the two terminal carbons, and the KIE should be maximum. Inspection of the mPW1K/6-31+G(d,p) transition state geometry (Figure 2a) reveals, however, that the terminal carbons and the transferred hydrogen are not collinear: $\angle_{CHC} \approx 134°$. This non-collinear geometry means that the transferred hydrogen moves with an unusually high frequency compared to the symmetric stretch of the linear transition state where H (D) does not move. Thus, coupling of the stretching and out-of-plane bending modes at the transition state partially offsets the zero-point contribution from the reaction coordinate and diminishes the KIE.[35] How much does the ZPE change? Figure 3 shows the changes in the bound normal modes orthogonal to the MEP as a function of the distance along the reaction path.

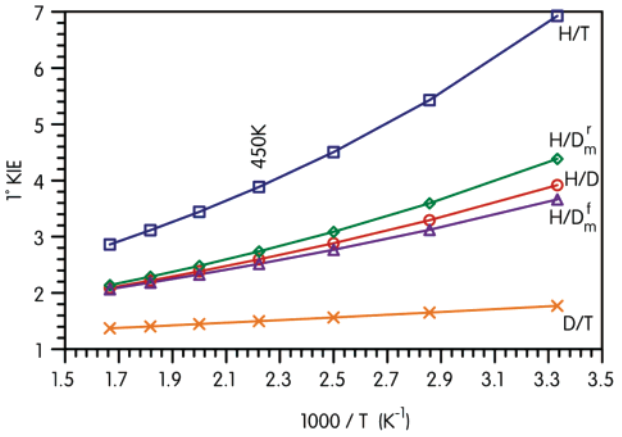

FIGURE 1. Calculated primary H/D, H/T, and D/T KIEs. m = Roth's mixed labeling experiment, f = forward reaction, r = reverse reaction. H/T = k_{HHHHH}/k_{THHHH}, H/D = k_{HHHHH}/k_{DHHHH}, $(H/D)_m^f = k_{HHHDD}/k_{DDDHH}$, $(H/D)_m^r = k_{HDDHH}/k_{DHHDD}$, D/T = k_{DHHHH}/k_{THHHH}.

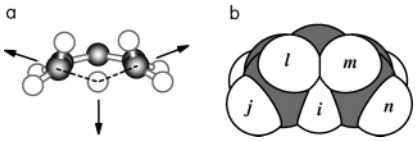

FIGURE 2. The mPW1K/6-31+G(d,p) transition state: (a) showing non-collinear CHC atoms and the associated displacement vectors for the symmetric stretch, and (b) the space-filling model showing compression of nonbonded hydrogens.

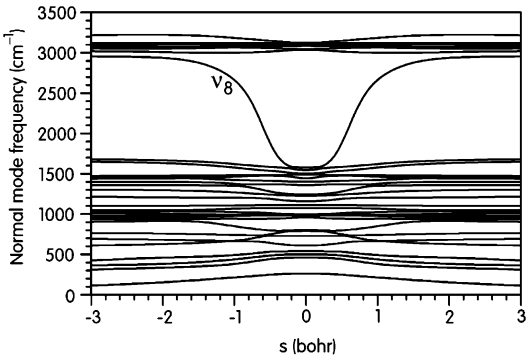

FIGURE 3. Normal-mode frequencies along the reaction coordinate *s*.

(32) Jursic, B. S. *J. Mol. Struct.* **1998**, *423*, 189. Saettel, N. J.; Wiest, O. *J. Org. Chem.* **2000**, *65*, 2331.
(33) Jaio, H.; Schleyer, P. v. R. *J. Chem. Soc., Faraday Trans. 1* **1994**, *90*, 1559.
(34) Zhang, Q.; Bell, R.; Truong, T. N. *J. Phys. Chem.* **1995**, *99*, 592. Baker, J.; Muir, M.; Andzelm, J.; Scheiner, A. *ACS Symp. Ser.* **1996**, *629*, 342. Skokov, S.; Wheeler, R. A. *Chem. Phys. Lett.* **1997**, *271*, 251.
(35) Westheimer, F. H. *Chem. Rev.* **1961**, *61*, 265.

TABLE 1. Quasiclassical Secondary H/D KIEs for the [1,5] Hydrogen Shift

	isotopologues	KIE at 450 K	KIE at 300 K
1	k_{HHHHH}/k_{HDDHH}	0.99	0.96
2	k_{HHHHH}/k_{HHHDD}	0.96	0.90
3	k_{HHHHH}/k_{HDHHH}	1.02	1.03
4	k_{HHHHH}/k_{HHDHH}	0.97	0.93
5	k_{HHHHH}/k_{HHHDH}	0.97	0.92
6	k_{HHHHH}/k_{HHHHD}	0.99	0.97
7	k_{HHHHH}/k_{HDDDD}	0.95	0.86

In principle all modes contribute to the KIE, but the largest change occurs in mode ν_8, which drops from about 2960 to 1545 cm^{-1}.[36] Since mode ν_8 loses only about half its ZPE, the calculated quasiclassical KIE is reduced to approximately half the theoretical maximum. The diminished primary quasiclassical KIE for the [1,5] shift has important consequences for the interpretation of the experimental KIE. Additional normal-mode analyses for some representative isotopologues are provided in Figures S2 and S3.

Secondary KIEs. The initial secondary KIEs we calculated, namely the α substitution of deuterium at the terminal sp^3 carbon, showed an unexpected inverse secondary KIE (entry 1 of Table 1). The rehybridization from sp^3 reactant to sp^2-like transition state should result in a decrease in out-of-plane bending force constants and a normal KIE ($k_H/k_D > 1$). The reverse reaction (sp^2 to sp^3, entry 2, Table 1) shows the expected inverse KIE, but it is not obvious why one always gets an inverse KIE. Analysis of a space-filling model of the transition state (Figure 2b) however reveals the origin of this unusual secondary KIE. The mPW1K/6-31+G(d,p) distance between the two nonbonded secondary hydrogen nuclei l and m is only 2.08 Å, slightly less than the sum of two hydrogen van der Waals radii (2.27 Å). This compression of nonbonding hydrogens is a consequence of the suprafacial nature of the reaction and contributes to the large barrier (36.3 kcal/mol) of this reaction.[37] Steric compression *increases* the associated C−H out-of-plane bending forces, thereby canceling the expected *decrease* in out-of-plane bending forces expected for l as it rehybridizes from sp^3 toward sp^2. When l is deuterium, the reaction speeds up because deuterium is sterically less demanding; it has a narrower vibrational probability distribution due to its narrower zero-point motion.[38] Substitution of deuterium at just position j brings back the normal KIE because the outer position undergoes no bond compression but does rehybridize from sp^3 toward sp^2 (entry 3, Table 1). Substitution at m and n gives the usual inverse KIEs because both rehybridization effects and compression effects work in the same direction (entry 4 and 5, Table 1). The inverse nature of the secondary KIE has unusual consequences for the secondary Swain−Schaad exponents (supra infra).

Tunneling and Transmission Coefficients. Tunneling effects incorporated into the transmission coefficients are summarized in Table 2. The values for 300 K are given for reference; the reaction is too slow to measure at that temperature. Likewise, the one-dimensional tunneling coefficients (ZCT) are given for reference since the SCT more accurately models the experimental KIE. Note that even at elevated temperatures the tunneling effect is significant; it increases the rate of the perprotio isotopologue by nearly one order of magnitude. The table further indicates that neither D nor T are too heavy to tunnel, contrary to popular assumptions, and this has implications for the Swain−Schaad exponent.

TABLE 2. Transmission Coefficients for Various Isotopologues at Room Temperature and Experimental Temperatures

	κ (300 K)		κ (450 K)	
	ZCT	SCT	ZCT	SCT
HHHHH	22.7	691.9	3.0	9.0
DHHHH	5.8	75.9	1.9	4.4
THHHH	3.4	20.7	1.6	3.1
DDDHH	5.4	52.3	1.9	4.0
HDDHH	17.7	38.9	2.8	7.7
HTTHH	15.1	25.6	2.7	6.9
DTTHH	5.2	45.0	1.9	3.8

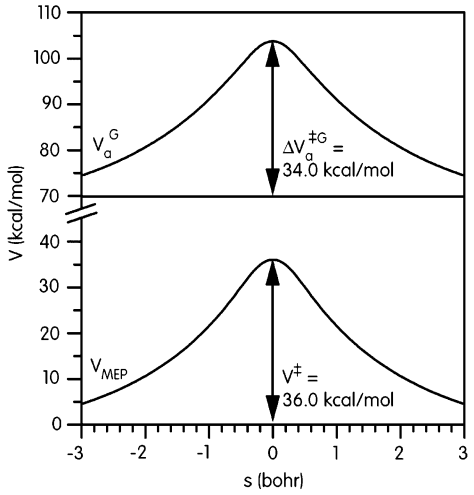

FIGURE 4. Born−Oppenheimer (V_{MEP}) and adiabatic (V_a^G) energies along the minimum energy path for the HHHHH isotopologue. The difference between the curves is the sum of the ZPE of vibrational modes orthogonal to the MEP. The zero of energy is the s-cisoid conformer. When the s-trans reactant is the zero of energy the potentials are about 3.3 kcal/mol higher (not shown).

Representative Tunneling Energies. The transmission coefficient is dependent on the tunnel path length. Near the top of the barrier, where the barrier is thinnest, the path is the shortest and the permeability is maximum. However, relatively few molecules have sufficient energy to explore the top of the PES. A Boltzmann distribution of kinetic energies ensures that more molecules explore the lower portion of the PES where the barrier is wider and tunneling is greatly diminished. One can define the most probable ("representative") tunneling energy (E_{rep}) as that energy that has the largest integrand in eq 6, $P(E)e^{-E/kBT}$, and thus contributes most to the transmission coefficient.[39] The potential energies and representative tunnel energies are shown in Figure 4 and Figure 5 and are summarized in the Table S4.

Although the E_{rep} decreases from H to D to T, the barrier heights ($V_a^{\ddagger G}$) for these isotopes decreases more rapidly, so that

(36) There are numerous avoided crossings in Figure 3 including one at about ±0.25 bohr between n_8 and a C=C stretching mode at ~1600 cm^{-1}. A diabatic correction allows one to smoothly connect these curves. Truhlar, D. G.; Isaacson, A. D. *J. Chem. Phys*. **1982**, *77*, 3516.

(37) The experimental barrier for the [1,7] shift is significantly lower (21.5 kcal/mol, Baldwin, J. E.; Reddy, V. P. *J. Am. Chem. Soc*. **1988**, *110*, 8223) in part because the non-transferred terminal hydrogens are well separated (3.51Å) according to the B3LYP/6−31G(d,p) transition state geometry.

(38) Melanders, L.; Saunders, W. H., Jr. R*eaction Rates of Isotopic Molecules*, 2nd ed.; John Wiley & Sons: New York, 1980; Chapter 6.

(39) Kim, Y.; Truhlar, D. G.; Kreevoy, M. M. *J. Am. Chem. Soc*. **1991**, *113*, 7837.

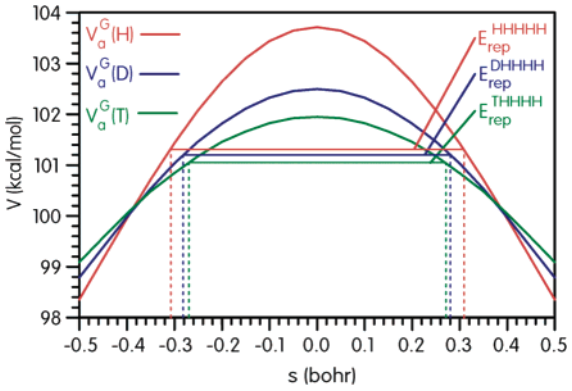

FIGURE 5. Expansion of V_a^G near the transition state for HHHHH, DHHHH, and THHHH showing how much of the barrier is evaded by tunneling. Horizontal lines associated with each curve are the SCT representative tunnel energies at 450 K and vertical lines are the associated turning points that define the most probable tunnel region.

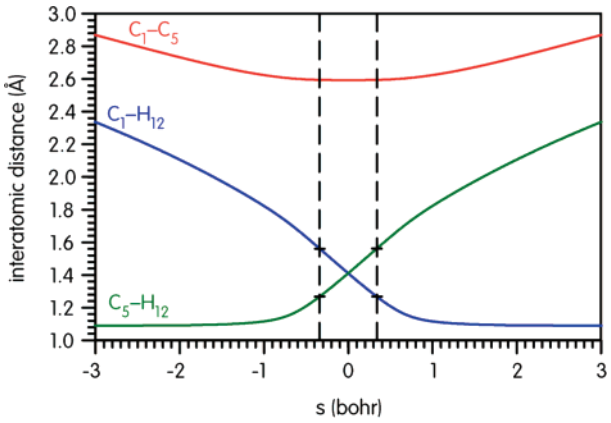

FIGURE 6. Interatomic distances (Å) along the minimum energy path. Dotted line represents turning points of E_{rep}(H) at 450 K.

heavier isotopes tunnel closer to their respective $V_a^{\ddagger G}$. In the experimental temperature range (450 K) H, D, and T "evade" about 2.4, 1.3, and 0.9 kcal/mol of the barrier, respectively. The associated tunnel paths are longer for lighter isotopes due to their greater de Broglie wavelength. Before the tunnel region is reached, most of the reaction involves the approach of the two terminal carbons with little change in the C_5-H_{12} distance (Figure 6). At about −1 bohr along the reaction coordinate the C_5-H_{12} distance begins to rise steeply as the C−H bond is broken and then increases more slowly after about +1 bohr. The carbon skeleton changes little in the tunnel region (C_1-C_5 interatomic distance constant at 2.59 Å), while the C_1-H_{12} distance undergoes significant changes.

Comparison of Tunneling Models. The excellent match between computed and experimental primary KIE (Figure 7) validates the SCT methodology. Not only is tunneling necessary to account for the observed KIE, one-dimensional models (zero curvature tunneling) are insufficient for describing the tunneling. Even semiempirical potentials gave reasonable primary KIEs (4.3−5.5) when SCT is used.[4] Thus, multidimensional tunneling is critical for accurate modeling of isotope effects in the [1,5] shift.

Unfortunately, the room-temperature rates for the [1,5] hydrogen shift are experimentally inaccessible. Doering and Zhao have extrapolated the room-temperature H/D KIE for 1,3-pentadiene to 8.9, but because of uncertainties in the Arrhenius

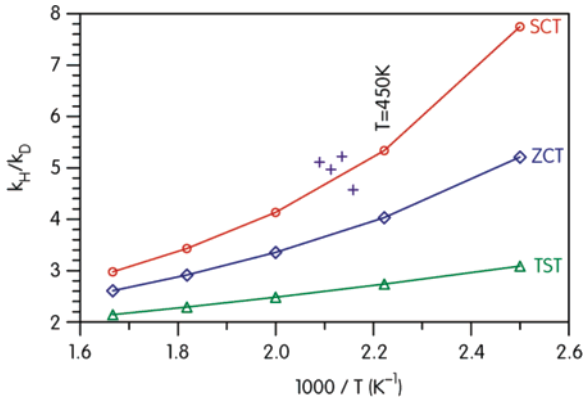

FIGURE 7. H/D KIE in the temperature range that coincides with the experimental temperature range. (+) represents Roth's experimental KIEs.[22]

parameters their computed KIE range is 2−54![2] Our prediction for the room-temperature KIE is closer to 32, owing to the steep temperature dependence of the SCT KIE in the low-temperature regime. In their work on the [1,5] H shift in 2-methyl-10-methylenebicyclo[4.4.0]dec-1-ene, Doering and Zhao challenge the theoretical community to identify the temperature range in which tunneling would become relevant to the experimentalist, where nonlinearity of an Arrhenius plot is apparently the only admissible evidence for tunneling.[2] We think that one does not need to look exclusively in the low-temperature regime for confirmation of tunneling; it is already present in the KIEs: without tunneling the KIE at 470 K should be 2.6, yet both the experimental KIE (∼5) and SCT calculated KIE (4.8) are significantly higher (Figure 7) due to the presence of tunneling, which increases k_H by one order of magnitude (Table 2). An experimental KIE with a low magnitude is not sufficient evidence for the absence for tunneling. Additionally, we have established the accuracy of the multidimensional tunneling model in predicting KIEs for this reaction and can now proceed to consider tunnel effects on secondary KIEs and SSEs with confidence in the method.

Tunnel Effects on Secondary KIEs. Tunneling perturbs the quasiclassical secondary KIEs as shown in Table 2 and Figure 8. α-Secondary KIEs should vary from unity for reactant-like transition states to near the equilibrium isotope effect (EIE, dashed line in Figure 8) for product-like transition states[40] unless the KIE is perturbed by tunneling.[41] The EIE is determined primarily by the isotope effect on the hydrogen transfer step but also includes the small contribution of isotopes on the s-trans/s-cis pre-equilibrium. The EIE is greater than unity in the forward direction (k_{HDDHH}, Figure 8a) and less than unity in the reverse direction (k_{HHHDD}, Figure 8b) because deuterium prefers to occupy the site with the lower zero-point energy, i.e., deuterium at the sp^2 carbon. The nontunneling (TST) KIE is inverse for both the forward and reverse reaction due to the steric compression effects noted above. Inclusion of tunneling along the MEP (ZCT) converts an *inverse* KIE to a *normal* KIE. Traditionally, KIE > EIE has been interpreted as evidence for

(40) Melander, L.; Saunders, W. H., Jr. *Reaction Rates of Isotopic Molecules*, 2nd ed.;Wiley: New York, 1980. Saunders, W. H., Jr. In *Investigation of Rates and Mechanisms of Reactions*, 4th ed.; Bernasconi, C. F., Ed.; Techniques of Chemistry, Vol. VI, Part 1; Wiley & Sons: New York, 1986; p 565.

(41) Pu, J.; Ma, S.; Garcia-Viloca, M.; Gao, J.; Truhlar, D. G.; Kohen, A. *J. Am. Chem. Soc.* **2005**, *127*, 14879.

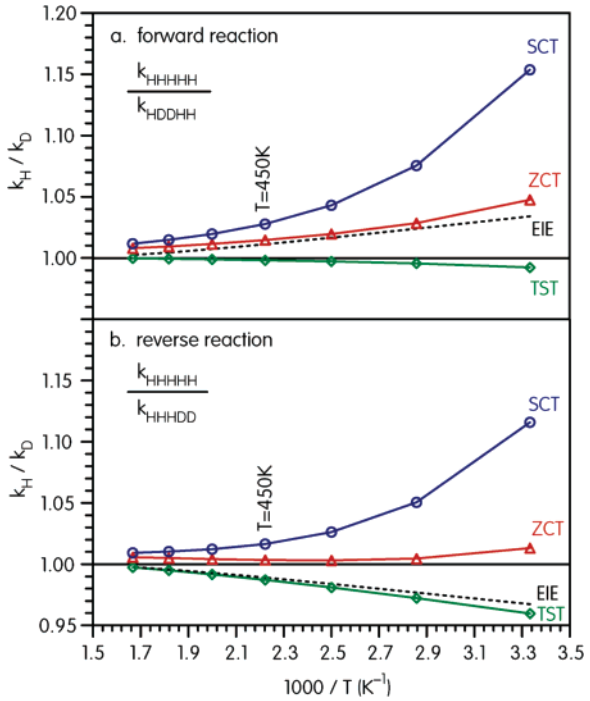

FIGURE 8. Temperature and model dependence of the secondary H/D KIE: (a) forward reaction, k_{HHHHH}/k_{HDDHH}, (b) reverse reaction, k_{HHHHH}/k_{HHHDD}. Solid curves are KIEs, the dashed line is EIE, equilibrium isotope effect. The horizontal line at $k_H/k_D = 1$ separates normal from inverse KIEs. The difference between any two curves in the forward direction is identical to difference in the reverse direction because the transmission coefficient is the same in both direction.

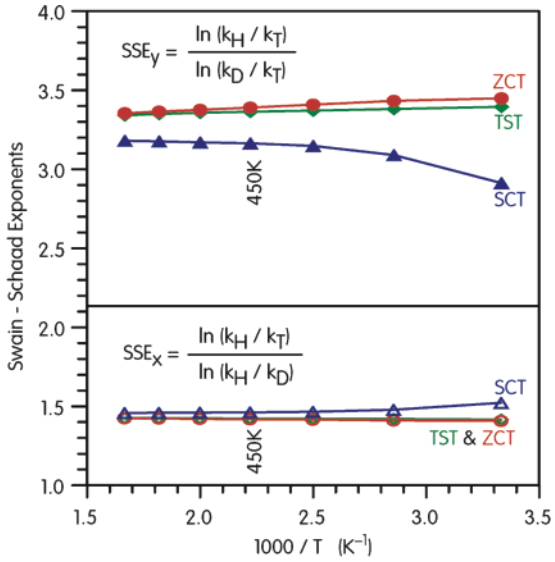

FIGURE 9. Primary Swain−Schaad Exponents for different models at different temperatures.

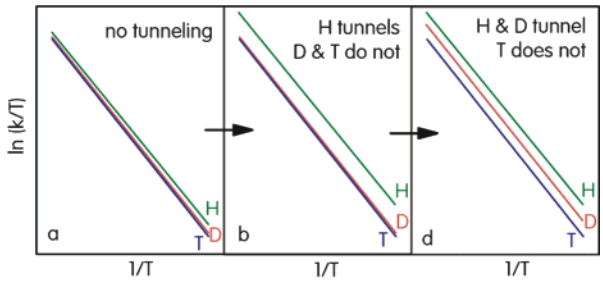

FIGURE 10. Hypothetical Eyring curves for different isotopes with and without tunneling.

tunneling and specifically coupled motion of bending modes with tunneling along the reaction coordinate. The multidimensional tunneling (SCT), which specifically allows for these couplings, shows that the KIE moves further into the "normal" range and approaches a value of 1.15 in the temperature range where kinetics are easily measured (450 K). Even relatively insensitive techniques such as NMR can distinguish KIEs as small as 1.15.[42] Compared to the H/D KIEs, the secondary H/T and D/T KIEs are larger and smaller in magnitude, respectively, but otherwise show the same qualitative behavior (Figures S6 and S7).

Primary Swain−Schaad Exponents. The primary Swain−Schaad exponents depicted in Figure 9 display a number of features typical of these exponents: they are largely temperature independent, the *y* exponents are larger in magnitude than the *x* exponents, tunneling inflates one exponent but deflates the other,[43] and tunneling perturbs the primary Swain−Schaad exponents by amounts too small to be experimentally distinguished, e.g., $y_{TST}^{450K} = 3.36$ vs $y_{SCT}^{450K} = 3.16$.

These results are in qualitative agreement with Borden's results on 5-methyl-1,3-cyclopentadiene:[24] in the experimentally accessible temperature range, tunneling does not have a large effect on the primary SSE. However, we do not see an inflated *y* exponent in the range of 300−600 K nor any indication of a crossover point. There are a few examples in which tunneling deflates the *y* exponents[10,11] but as yet no experimental observation of a deflated *y* SSE. What factors govern inflation and deflation of the SSE? The phenomenon can be understood through the hypothetical Eyring plots in Figure 10.

The KIE is related to the distance between any two lines of an Eyring plot; the larger the separation, the greater the KIE. The SSE on the other hand is related to the relative position of the middle (deuterium) curve. Because of its relative reduced mass, the quasiclassical deuterium curve lies closer to tritium's curve (Figure 10a). If only protium tunnels significantly (Figure 10b), the D curve moves further from H and *relatively* closer to T. This will *always* lead to inflation of the *y* exponent. If only H and D tunnel significantly (Figure 10c), the D curve moves relatively closer to the H curve, provided κ_H is not drastically greater than κ_D. This will *always* lead to deflation of the *y* exponent. In a more realistic scenario all three isotopes tunnel, as seen in the Eyring plots calculated with the TST and SCT methods (Figure 11) and in the transmission coefficients (Table 1).

Tunneling raises all three curves and spreads them further apart with greater spread at low temperatures. One can even detect slight curvature at low temperature for the lighter isotopes, although such non-Arrhenius behavior would be difficult to detect experimentally. More significantly, the deuterium curve occupies a position relatively closer to the middle, and by the analysis above, results in a deflated *y* exponent. According to Figure 9 this is a feature of the SCT method, since the ZCT inflates the *y* exponent slightly. Thus the inflation or deflation of the SSE depends critically on accurate calculation of the

(42) Perrin, C. L.; Thoburn, J. D.; Kresge, A. J. *J. Am. Chem. Soc.* **1992**, *114*, 8800.

(43) It is readily shown that the sum of the reciprocal of the exponents is unity, i.e. that $1/x + 1/y = 1$. Therefore, if *x* increases, *y* must decrease.

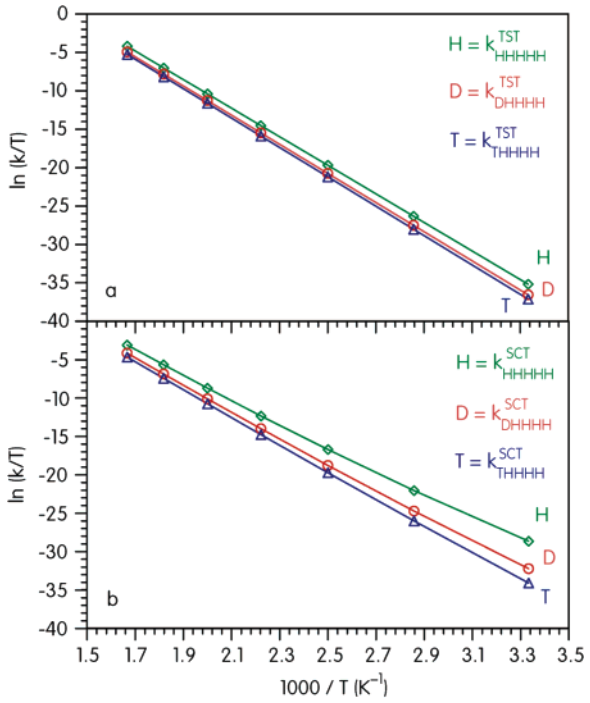

FIGURE 11. Eyring plots showing the effects of tunneling on the rates of individual isotopes. (a) Quasiclassical (no tunneling), linear Eyring plot. (b) Small-curvature tunneling Eyring plot showing that D occupies a more middle position resulting in a deflated y exponent.

transmission coefficients. Based on the agreement between the SCT primary KIE and the experimental KIE, we believe the SCT model is superior to any of the one-dimensional models, and thus predict a deflation of the *y* exponent relative to the quasiclassical *y* exponent.

The aforementioned prediction is, of course, determined by the PES, and thus limited to this particular reaction. Still it would be useful to generalize this result to other reactions. Under what general conditions is the Swain−Schaad exponent deflated? Inclusion of tunneling in eq 1 via transmission coefficients leads to eq 7

$$y_{QMT} = \frac{\ln\left(\frac{\kappa_H}{\kappa_T}\frac{k_H}{k_T}\right)}{\ln\left(\frac{\kappa_D}{\kappa_T}\frac{k_D}{k_T}\right)} \quad (7)$$

where QMT, quantum mechanical tunneling, is any of the tunnel methods: Bell, ZCT, or SCT. Rearrangement gives a relationship between the quasiclassical exponent (y_{TST}) and the tunneling exponent (y_{QMT}):

$$y_{QMT} = \frac{y_{TST} + \frac{\ln(\kappa_H/\kappa_T)}{\ln(k_D/k_T)}}{1 + \frac{\ln(\kappa_D/\kappa_T)}{\ln(k_D k_T)}} \quad (8)$$

Thus, the SSE with tunneling scales with the magnitude of the D/T KIE, the transmission coefficient ratios, and the quasiclassical SSE, which is effectively constant (Figure 9). When the transmission coefficient ratios are allowed to vary independently, as they might for different reaction types, a plot

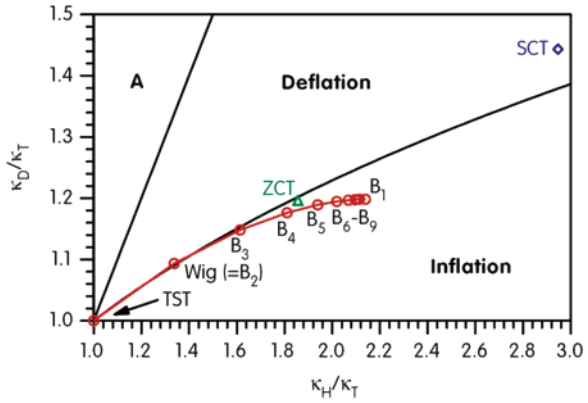

FIGURE 12. Inflated and deflated regions of the Swain−Schaad with location of transmission coefficient ratios for various tunneling models at 450 K.

with various inflated and deflated regions is generated upon which specific κ ratios can be superimposed (Figure 12). Data points further from the origin represent larger tunnel contributions and larger KIEs. The curve demarcating the inflated and deflated regions represents the special case where $y_{TST} = y_{QMT}$ and is calculated according to

$$\frac{\kappa_D}{\kappa_T} = e^{(\ln(\kappa_H/\kappa_T)/y_{TST})} \quad (9)$$

This line represents the case where tunneling is occurring (κ not unity), but the SSE exponent will not detect the tunneling because of fortuitous κ ratios. This is a known limitation of the SSE.[6,10] The line demarcating region A and the deflated region has a slope of unity and represents the case where $\kappa_D/\kappa_T = \kappa_H/\kappa_T$, in other words when $\kappa_H = \kappa_D = \kappa_T$. Note that there are no data points near that line. In region A, κ_D/κ_T is greater than κ_H/κ_T, leading to the even more unusual result that $\kappa_D > \kappa_H$ (D tunnels more than H!). There are in fact cases where deuterium tunnels more than protium;[10,44] however, they tend to occur when the barriers are small, so that the protium with its higher ZPE preferentially crosses the classical barrier, while deuterium explores a lower and wider portion of the potential where it can take advantage of tunneling paths. Note that all of the calculated data for the [1,5] shift fall nearer $y_{QMT} = y_{TST}$ but on both sides of it. Data further from the demarcation curve represent greater in-/de-flation.

Is the deflated SSE predicted by the SCT model an artifact of the multidimensional nature of the model? One-dimensional models qualitatively reproduce the KIEs, but do they also reproduce the trend in the SSE? Figure 12 shows that while the SSE based on the two-term Bell (Wigner) model lies just inside the deflated region, all other Bell SSEs lie progressively further into the inflated region because they systematically overestimate tunneling in the lighter isotopes. The more accurate one-dimensional tunneling (ZCT) SSE still lies in the inflated region but much closer to the quasiclassical SSE. When multidimensional tunneling (SCT) is included the SSE moves into the deflated region. This indicates that tritium cannot keep up with protium and deuterium in the corner-cutting process (deuterium moves more toward the middle position in Figure 11), but in

(44) Truong, T. N.; McCammon, J. A. *J. Am. Chem. Soc.* **1991**, *113*, 7504. Storer, J. W.; Houk, K. N. *J. Am. Chem. Soc.* **1993**, *115*, 10426. Corchado, J. C.; Espinosa-Garcia, J. *J. Chem. Phys.* **1996**, *105*, 3160.

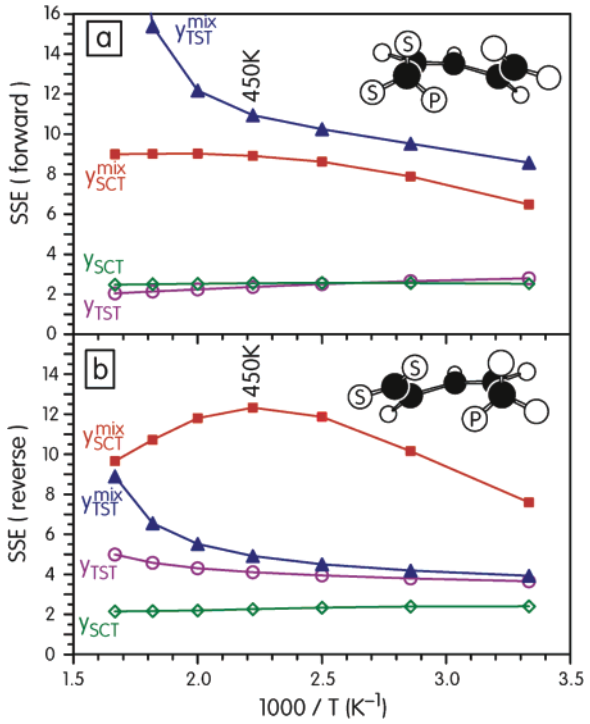

FIGURE 13. Temperature and model dependence of secondary Swain−Schaad exponents for (a) the forward and (b) reverse reaction. S = H, D, or T at secondary position. P = H or D at primary position.

the one-dimensional ZCT model tritium can. This shows again the importance of multidimensional tunneling in modeling the [1,5] shift. However, even SCT-induced deviations in the SSE are still be too small to be observed experimentally and so we consider next the secondary SSEs.

Secondary Swain−Schaad Exponents. Figure 13a shows that the secondary Swain−Schaad exponent y_{TST} derived from the forward reaction (heavy isotopes at α-secondary sp^3 carbon) does not show a large temperature dependence, even when tunneling is present (y_{SCT}). Depending on the temperature, tunneling could increase or decrease the SSE but not significantly in either case. In fact, the crossover point is near the experimental temperature range, rendering that secondary SSE completely ineffectual at detecting the tunneling that is clearly present ($\kappa_H^{450K} = 9.0$). When the specific ("mixed") isotopic substitution pattern

$$y^{mix} = \frac{\ln(k_{HHHHH}/k_{HTTHH})}{\ln(k_{DDDHH}/k_{DTTHH})} \qquad (10)$$

is considered, the quasiclassical SSE increases substantially (from 2.4 to 10.9). More importantly the mixed SSE is more sensitive to tunneling effects but again does *not* show the anticipated inflation ($y_{TST}^{mix} = 10.9$ and $y_{SCT}^{mix} = 8.9$). Likewise, the reverse reaction (Figure 13b) shows a deflated SSE ($y_{TST} = 4.1$ and $y_{SCT} = 2.3$ at 450 K) unless mixed labels are used, in which case the SSE is substantially inflated ($y_{TST}^{mix} = 4.9$ and $y_{SCT}^{mix} = 12.3$). In summary, tunneling can inflate and deflate SSEs by either large or small amounts, with the reverse reaction showing the greatest affect. Although the effects of tunneling on the secondary SSE appear quite variable, the secondary SSE would be capable of detecting tunneling, provided the correct labeling scheme is chosen. While the mixed secondary labeling schemes give the largest differences, mixed labeling does not appear to be a requirement for detection of tunneling, if one can obtain accurate KIEs. The mixed secondary SSE presented above is for heavy isotopes at both α-secondary positions. When only the "inside" α-position is substituted, the graphs are qualitatively similar (Figure S8), except that the TST curves are lowered. In these cases tunneling now results in an inflated SSE because y_{TST} has dropped. When the "outside" position is substituted, the SCT exponents are fairly stable, but the QC exponents reach an asymptote (Figure S9).

The variability of the quasiclassical SSE arises from secondary D/T KIEs that are close to unity. The effect is more pronounced at high temperatures because the KIE approaches 1 at high temperature. The instability of the QC SSEs under certain conditions was first noted by Stern[45] and emphasized by Singleton.[13] Why do the tunneling models not show this instability? As depicted in Figure 8, tunneling contributions move the inverse quasiclassical secondary D/T KIE well into the "normal" range, away from the conditions that cause anomalous behavior (k_D/k_T approaching unity). In this case the H/T and D/T KIEs remain in the normal range where their ratio is little changed.

Abstraction of hydrogen from benzylamine by bovine serum amine oxidase shows a significant primary KIE (∼10−20) but no significant secondary KIE (∼1.2) nor an unusual mixed secondary SSE (∼3−4) because the primary and secondary hydrogen motions are largely decoupled.[46] When primary and secondary motions are coupled as in the enzyme-catalyzed hydrogen abstraction from benzyl alcohol by nicotinamide cofactors, the secondary SSE is either "normal" or inflated depending on how successfully mutants are at unmasking tunneling effects.[17] Interestingly, these enzymatic reactions never appear to deflate SSEs, perhaps because the substitution pattern that gives deflation in the pentadiene is not the exact substitution pattern of benzyl alcohol substrate used in the ADH studies. When the substitution patterns are similar, the predicted pentadiene mixed secondary SSEs (8.3−10.8) compares favorably with the SSE for wild type ADH oxidations of benzyl alcohol (9.9−10.2).[47] The mixed secondary SSE is very sensitive to the location of the heavy isotopes.

Singleton concludes that secondary SSE, although more sensitive than primary, will only be useful indicators of tunneling if the H/T KIE is sufficiently large *and* the SSE is sufficiently unusual. On the basis of our multidimensional tunneling calculations, we predict an H/T KIE of 1.28 and a secondary SSE of 2.26 (both at 450 K), which are outside the range defined by Singleton, i.e., secondary KIEs outside the range $0.9 < k_H/k_T < 1.1$ and secondary SSE outside the range $2.95 < SSE < 4.52$.[48] In other words, if the experimental SSE is near our predicted value, its magnitude *is* sufficient to indicate tunneling. This entire analysis is rather complex and relies upon analogy with model compounds. We feel it is simpler to directly compare y_{TST} with y_{SCT} (4.1 vs 2.3, or 4.9 vs 12.3, if mixed isotopes are used). These values may be sufficiently different to be distinguished experimentally. The strength of this line of argument

(45) Stern, M. J.; Vogel, P. C. *J. Am. Chem. Soc.* **1971**, *93*, 4664. Stern, M. J.; Weston, R. E. *J. Chem. Phys.* **1974**, *60*, 2803, 2808, 2814.
(46) Grant, K. L.; Klinman, J. P. *Biochemistry* **1989**, *28*, 6597.
(47) Note however that a subtle change in substrate, from benzyl alcohol to *p*-methoxybenzyl alcohol, reduces the yeast−ADH-catalyzed secondary y^{mix} to the normal range (2.8 ± 0.8). Rucker, J.; Cha, Y.; Jonsson, T.; Grant, K. L.; Klinman, J. P. *Biochemistry* **1992**, *31*, 11489.
(48) These minima and maxima are determined according to $3.40 - 0.13/(k_H/k_T - 1)$ for the minimum and $3.66 + 0.24/(k_H/k_T - 1)$ for the maximum according to reference 13.

relies on the accuracy of the quasiclassical KIE, which in turn is primarily a function of the vibrational frequencies. While systematic errors are expected in all calculations (and experiments), comparison of two calculated quantities, e.g., k_H/k_D or $\ln(k_H/k_T)/\ln(k_D/k_T)$, will always be more reliable due to partial cancelation of those errors. Given the reliability of calculated ZPE and our success at modeling experimental KIEs with small curvature tunneling, we believe we can predict both the KIE and the SSE reasonably well.

While SSE experiments could be useful in detecting tunneling, the extra labeling experiments required to measure the SSE may be redundant. A simpler experiment requires merely the measurement of secondary H/D KIE. As noted above (Figure 8) tunneling converts the inverse secondary KIE into a normal secondary; thus, to verify tunneling, one need only determine whether deuterium substitution at a secondary position retards the [1,5] shift (quasiclassical behavior) or enhances it (tunneling behavior).

Concluding Remarks

Comparison of the quasiclassical and SCT rates for [1,5] hydrogen shift in pentadiene indicates that multidimensional tunneling is needed to account for experimental KIEs. One-dimensional tunneling models give a quantitatively different KIE and very different primary SSE behavior, namely inflation rather than deflation. Inflation and deflation of the secondary SSE is more complex and depends on temperature and direction of reaction. If the heavy isotopes are strategically placed, the secondary SSE could be a useful diagnostic for quantum tunneling. For pentadiene, however, the extra tritium labeling experiments required to measure an SSE probably would not reveal anything new because the tunneling would already be apparent in primary H/D KIEs (an experimental value near 5.2 vs a value of 2.5 expected for a quasiclassical KIE), as well as in the secondary H/D KIEs ("normal" for SCT, but "inverse" according to quasiclassical predictions). The universality of these conclusions, however, is not guaranteed because so many other factors including coupled motions, position of transition state, kinetic complexity, and modulation of environment may affect tunneling in other reactions. We plan to explore the SSE of other reactions with this methodology to see how general these conclusions are. Of special interest is to see how asymmetry might reduce the tunneling. The requisite calculations are readily accessible for small organic compounds. Truhlar and co-workers have demonstrated that they are doable even for larger enzymatic systems.[49]

While some have questioned the need to invoke tunneling in the [1,5] shift, we find that KIEs and Swain−Schaad exponents are all capable, in principle, of detecting tunneling even though the tunneling contributions are only "moderate". Our test for tunneling is not limited to finding the incontrovertible temperature-independent regime where tunneling dominates. We suggest that a more fruitful approach starts with the acknowledgment that hydrogen tunneling is a ubiquitous (but not necessarily universal) feature of hydrogen transfer. The operative question for both experimentalist and theoreticians is then to determine the extent of tunneling along the subtle continuum of tunneling regimes.

Acknowledgment. We thank Prof. D. Truhlar for providing the POLYRATE9.4 and GAUSSRATE9.4 programs and helpful discussions regarding its implementation. This work was supported in part by a Chenery Research Professorship to J.D.T.

Supporting Information Available: Computation details, coordinates and energies of all stationary states at the mPW1K/6-31+G(d,p) level of theory, potential energy surface, normal-mode analysis, transmission coefficients, representative tunneling energies, rates, secondary kinetic isotope effects, secondary Swain−Schaad exponents, and Arrhenius activation parameters. This material is available free of charge via the Internet at http://pub.acs.org.

JO702668U

(49) Truhlar, D. G.; Gao, J.; Alhambra, C.; Garcia-Viloca, M.; Corchado, J.; Sanchez, M. L.; Villa, J. *Acc. Chem. Res.* **2002**, *35*, 341. Pu, J.; Gao, J.; Truhlar, D. G. *Chem. Rev.* **2006**, *106*, 3140.